

Uncertainty quantification for advanced progressive damage models for composites by means of efficient emulators and bootstrapping

Giuseppe Catalanotti

*Escola de Ciências e Tecnologia, Universidade de Évora, Colégio Luis António Verney,
Rua Romão Ramalho 59, 7000-671 Évora, Portugal*

School of Mechanical and Aerospace Engineering, Queen's University Belfast, Belfast, BT9 5AH, UK

Abstract

A methodology was developed and validated to quantify the uncertainty for advanced progressive damage models for composites. It relies on a pragmatic approach entailing the definition of efficient emulators, the use of state-of-the-art computational models, and the employment of bootstrapping statistic techniques. The proposed methodology was calibrated on numerical results obtained running a limited amount of virtual experiments (five for each configuration) of unnotched and open-hole specimens in tension and compression. The structural strength was taken as the quantity of interest, and a methodology was proposed and validated to determine its distribution and associated statistics.

Keywords: Statistical properties/methods, Analytical modelling, Computational modelling, Strength

1. Introduction

Advanced Finite Element Analysis (FEA) tools for composite materials (based on Cohesive Elements [1–7], Continuum Damage Mechanics [8–11], Discrete Damage Modeling [12, 13], Smeared Crack Model [14, 15], among others) permit the modelling of inter- and intra-laminar damage and thus allow the behaviour of complex material systems to be simulated at micro- [16, 17], meso- [18], and macro-scales [19]. These computational models are state-of-the-art, the result of years of research and collaboration between the aerospace industry and academia, and represent the most powerful tools that engineers have available.

Email address: gcatalanotti@uevora.pt (Giuseppe Catalanotti)

Physical experiments are necessary for characterisation, validation, and certification purposes. Apart from the elastic properties, the use of the aforementioned computational models require the definition of the softening laws or, in other words, the experimental determination of the strength and fracture toughness (or resistance curve) associated with each failure mechanism. While determining the strength is a common (often standardised) practice, measuring the fracture toughness is more complex since standardised test methods exist for interlaminar fracture toughness (i.e. delamination) but not for intralaminar. Hence, the need to propose test methods for intralaminar fracture toughness adapting test methods available for metals ([20], among others) or extending the size effect method [21–23] to composite laminates. Recent developments in characterisation experiments have been focusing on defining methodologies to measure the intralaminar fracture toughness at extreme loading scenarios [24–27] and on quantifying uncertainty for different loading conditions [28]. Recent advances in experimental mechanics, especially in full-field optical techniques [29, 30], have created conditions for the establishment of new experimental protocols, which, when used with current standardised procedures, allow the collection and analysis of a significantly larger set of valuable experimental data and allow the reduction of the uncertainty of the experimental measurement.

If the numerical input parameters (material properties, geometry, and boundary conditions) are considered deterministic values, as normally done, the output of the computational model will be deterministic. Comparing this deterministic numerical prediction with the result of a validation experiment says little about the agreement between the two, and does not allow for a proper assessment of the performance of the computational model. In turn, this detracts engineers from using it confidently, either for calibration purposes, to explore the design space, or to optimise the system under consideration. Model evaluation can only be done correctly if its input parameters are considered stochastic values and if an Uncertainty Quantification and Management (UQ&M) analysis is performed.

A proper UQ&M framework should include the following tasks [31]:

- The quantification of the sources of uncertainty, which will provide an appropriate probabilistic description for the input parameters, and whose result will consist of a random vector of input parameters that will be fed into the computational model;
- The propagation of uncertainty, which will allow the determination of the Quantity of Interest (QoI) in a statistical manner (e.g. moments of the output distribution, probability

of failure, response probability distribution function);

- A sensitivity analysis (or Bayesian inversion) which will allow the knowledge of the uncertainty of the input parameters to be updated. This step provides valuable information that can support the decision of either i) attempting to reduce the variability of the input parameter by e.g. performing additional experimental tests, or ii) discarding its importance and reducing the dimensionality of the problem.

Monte Carlo Simulation (MCS) is a well-known technique that allows the propagation of uncertainty throughout the sampling of input variables and computation of the corresponding output. Although the technique is well-posed and convergence is ensured, the main issue with MCSs is that they usually require 10^4 – 10^5 runs to converge, and 10^6 – 10^7 runs to perform a proper sensitivity analysis [31]: far too many for the computational models under consideration, since each run would require several hours of computational time. Hence, there is a need to resort to the use of emulators (also called surrogate models, metamodels, or response surfaces).

An emulator reproduces the original computational model. It is calibrated on limited runs of the original model (hereinafter denoted *calibration runs*) and can be executed with negligible computational effort.

Therefore, to define an emulator, it is necessary [31]:

- To run the original computational model for selected values of the input vector chosen using different sampling techniques (e.g. Latin Hypercube Sampling);
- To choose a proper class (i.e. functional shape) for the meta-model (e.g. polynomial chaos expansion [32], low-rank tensor approximations [33], kriging [34], support vector machines [35], neural networks, etc.)
- To calibrate the emulator with the generated data, by using the original computational model. This is achieved using different techniques, such as full quadrature [36], sparse grid integration [37], least-squares analysis [38], compressive sensing [39], etc., depending on the functional shape chosen for the emulator.
- To propagate uncertainty by applying MCS to the emulator to derive the statistical properties of the QoI.

Although a lot of research has recently been done to propose more advanced UQ&M methods for engineering problems, only a few are the examples of them being applied to strength

analysis methods for composites that use analytical [40] or numerical [41] tools requiring negligible computational effort, thus making the execution of hundreds or thousands of calibration runs perfectly acceptable.

But the FEA computational models taken as the benchmark in the aerospace industry and academia are much more complex (they take into account several damage mechanisms) and extremely time-consuming: running them, even a dozen times, is not a viable option.

Is there a way to reduce the calibration runs to a bearable number suitable for an industrial environment? We will demonstrate that, for some cases, it is possible to answer positively to the previous question. We will achieve this result through a pragmatic approach entailing the definition of efficient emulators, the use of advanced progressive damage models for composites, and the determination of the stochastic response by means of appropriate statistical techniques.

2. Materials and methods

2.1. Definition of the emulator

The first step is to define an emulator that has to be fast and sufficiently precise. The aforementioned predictive computational models provide the mechanical behaviour of a structure in output. Although several variables can be monitored, the structural strength is the critical information that is retrieved and that is used for design purpose.

Therefore, the emulator will predict the strength of the structure, f , which depends on several stochastic variables necessary to define the material parameters, m_i , the orientation of the plies, θ_j , the geometric parameters, g_k , the loading, l_m , and the boundary conditions, b_n , and other additional variables:

$$f = f(m_i, \theta_j, g_k, l_m, b_n, \dots) \quad (1)$$

We assume the laminate to be a well-designed hard laminate subjected to an overall tensile/compressive stress. In this case the structural strength can be assumed to be dominated by the failure of the fibre. Therefore, a change in the strength of the ply X in the longitudinal direction or in the intralaminar fracture toughness associated with this failure mechanism \mathcal{G}_c will have a substantial effect on the strength of the laminate. A change on all the other material parameters, independently of their variability, has little effect on the strength of the laminate.

Considering also that manufacturing in the aeronautic industry heavily relies on automated systems (e.g. Automatic Tape Laying, Automatic Fibre Placement, etc.) the variability of the orientation of the plies, θ_j , and other geometrical parameters, g_i , can be neglected and the layup and dimension can be considered deterministic variables.

It should be considered that the aforementioned predictive models are employed during certification to speed up the process by replacing the physical experiments with virtual experiments. These models are used mainly on small structural elements (as open hole specimens, bolted joints, etc.) and never on full-scale models. These structural elements, having reduced dimensions, can be manufactured with very tight tolerance, and this circumstance further allows considering the geometric parameters, g_i , as deterministic variables.

Testing structural elements, for which standardised test methods exist, under controlled environmental conditions, permits also neglecting the variability of the loading, l_m , and boundary conditions, b_n , and allow considering these as deterministic variables.

Hence, there are only two stochastic variables, the ply strength X and the intralaminar fracture toughness \mathcal{G}_c . It is convenient to introduce a new stochastic variable $\lambda = X/\sqrt{\mathcal{G}_c}$ and to express the structural strength as depending on X and λ :

$$f = f(X, \lambda) \tag{2}$$

In an attempt to define an efficient emulator, let \bar{X} indicate a reference value of the strength corresponding either to its expected value, $E(X)$, or to the median, $X^{(50)}$ (hereinafter the p -th percentile of a stochastic variable will be indicated with p between two parentheses in superscript). When the ply strength is \bar{X} the structural strength can be calculated for some values of the ply fracture toughness, \mathcal{G}_c , to which correspond values of λ and f . Interpolating these values, e.g by using a PCHIP (Piecewise Cubic Hermite Interpolating Polynomial) interpolation, allows determining an approximation for the structural strength as a function of λ :

$$\Phi(\lambda) \approx f(\bar{X}, \lambda) \tag{3}$$

We now consider two similar softening laws (Fig. 1) with strength \bar{X} and X (we indicate with X either the stochastic variable or its realization). It is easy to demonstrate that similarity is ensured keeping a constant λ and this is true for triangular but also other softening laws

(e.g. the bilinear). It should be noted that for the same damage variable, $0 \leq d \leq 1$, the same percentage of fracture energy is dissipated in both cases.

We assume that at the peak load the two finite element models defined with the previous softening laws exhibit the same damage pattern (i.e. the i -th element in both FEM models will exhibit the same damage variable, d_i .) If this assumption holds, the structural strength scales with the ply strength, therefore it can be written:

$$\frac{f(X, \lambda)}{f(\bar{X}, \lambda)} = \frac{X}{\bar{X}} \quad (4)$$

hence, substituting (3) in (4) and rearranging yields:

$$f(X, \lambda) = \frac{X}{\bar{X}} \Phi(\lambda) \quad (5)$$

which completes the definition of the emulator.

Some assumptions made for the definition of the emulator may be too simplistic and not faithfully adherent to reality. Its accuracy might not be acceptable in some specific cases (e.g. soft laminates, exotic material systems, etc.) and needs to be assessed through experimental validation. However, the poor accuracy of the emulator does not hinder its usefulness for uncertainty quantification because it might still be employed (as crude as it is) in the framework of Multi Fidelity (MuFi) schemes which permit quantifying uncertainty by combining emulators with different levels of sophistication [42].

2.2. Computational model

For the calibration of the emulator, the computational model presented in [18] was used. This was able to simulate interlaminar and intralaminar damage and was able to predict with great accuracy (maximum relative error of 13%) different configurations used during the certification of aerospace-grade fibre-reinforced structural elements, including unnotched tension / compression, open hole tension / compression, and filled hole compression specimen. For conciseness, the details of the computational model are not reported here (since this is not the focus of this work), and the interested reader is referred to [18].

A portion of the virtual experiments run in [18], namely unnotched and open hole specimens made of IM7/8552 with $[0/90/-45/+45]_{3s}$ layup, were rerun here (Tab. 1). The material properties necessary to define the model, taken as deterministic variables, are reported in

Tab. 2. The only stochastic properties are the longitudinal strength and fracture toughness, in tension or compression, depending on whether the virtual experiment simulate a tensile or compressive case, respectively (see Tab. 3).

It is worth noticing that assuming a given distribution for these variables is not necessary for the definition of the emulator or to determine the statistics of the QoI through bootstrapping. However, in the following, a given distribution for strength and fracture toughness will sometimes be assumed for the sake of discussion. When this will be deemed necessary, strength and fracture toughness will be considered to have log-normal distribution. This is preferred to the abused normal distribution simply because strength and fracture toughness are non-negative variables and, therefore, a distribution with support in $[0, +\infty]$ seems more appropriate. Hence, strength and fracture toughness read:

$$X = \exp(\mu_X + \sigma_X Z_1) ; \quad \mathcal{G}_c = \exp(\mu_G + \sigma_G Z_2) \quad (6)$$

where Z_1 and Z_2 are standard normal variables and μ_i and σ_i are the scale and shape parameters that are calculated in Tab. 3.

2.3. Statistical analysis

The distribution of the strength and fracture toughness are essentially unknown. The design engineers rely only on a limited number of experiments (i.e. realizations) and have no solid grounds to estimate the said distributions. Performing additional experiments is not viable because it does not necessarily solve the problem and is quite costly. Hence, design engineers need to work with the few experimental data they have available and must make the best use of them.

Considering these circumstances, bootstrapping seems to be the natural choice to construct an estimator for the desired parameters of the distribution of the QoI. Bootstrapping is a statistical technique that uses random sampling with replacement. It was proposed for the first time in [43] and since then has been expanded and used in different fields [44]. Bootstrapping does not require the knowledge of the distribution of the strength and fracture toughness and is particularly convenient, in this case, because permits analysing different groups of sample data without the burden of performing additional experiments.

The QoI can be any: the mean value of the structural (i.e. the strength of the specimen), its variance, or any other additional statistical parameter. Due to the importance given by the

designers in the aerospace field, the parameter that will be determined is the so-called A-basis value, i.e. the strength at which only 1% of the specimens will fail with a 95% confidence level.

The procedure used will be the following (Fig. 2):

- Assuming that there are n_X experimental values for the strength and n_G experimental values for the fracture toughness, and denoting by $n_{Max} = \max(n_X, n_G)$, two bootstrap samples of length n_{Max} , are generated for the strength and the fracture toughness, respectively. This allows forming n_{Max} couples, each containing a strength and a fracture toughness value.
- Each couple, given as input to the emulator of Eq. (3) will provide a value of the structural strength, allowing the determination of the empirical probability distribution of the structural strength.
- This procedure is repeated $N = 1000$ times (MCS) and this will allow one to obtain N distributions of the structural strength.
- At this point, theoretically, the first percentile (necessary for the determination of the A-basis value) could be directly determined from the empirical distribution. It is well known, however, that bootstrap is able to determine the statistic that characterises the centre of the distribution (mean, median, variance), but usually fails when used to estimate extreme values, such as extreme percentiles. To solve this issue, it was decided to determine the best fit of the empirical distribution and to use the latter for the determination of the first percentile of the structural strength. To avoid assuming any functional form of the distribution (i.e. avoiding "making up" the distribution), kernel density estimation (KDE) was used. Considering that the bandwidth of the kernel also affects the fitting, this is not imposed but chosen through optimisation, via grid search cross-validation [45], of the log-likelihood of the test data in the estimated density.
- The KDE fit of each strength distribution allows one to determine for the i -th iteration the corresponding value of the first percentile, $f_i^{(1)}$. These values are then collected and the distribution for the first percentile of the strength $f^{(1)}$ is generated. Finally, the

A-basis value is obtained by computing the 5th percentile of this distribution¹.

3. Calculations and Discussion

3.1. Preliminary calculations

The emulator's definition requires some assumptions whose suitability can be assessed by comparing the emulator's and the computational model's predictions.

Preliminary simulations of unnotched and open-hole specimens were conducted to assess the validity of Eq. (4). Simulations were carried out for the tensile specimens UT, OHT12, OHT60 and for the compressive specimens UC, OHC12, OHC30 (Tab. 1). The strength and fracture toughness were assumed to follow log-normal distributions with parameters reported in Tab. 3. The reference value of the strength, \bar{X} , was taken as the median value of the strength distribution, $\bar{X} = X^{(50)} = \exp(\mu_X)$, while λ was taken constant and equal to $\lambda = X^{(50)}/\sqrt{\mathcal{G}_c^{(50)}} = \exp(\mu_X - \frac{\mu_{\mathcal{G}}}{2})$. Simulations were carried out for different values of the strength X in the interval $[X^{(0.1)}, X^{(99.9)}]$ and the error made using Eq. (4) was computed (Fig. 3). The error was found to be smaller than 10% (in absolute value) in the interval $[X^{(0.1)}, X^{(99.9)}]$ and smaller than 2% in the interval $[X^{(10)}, X^{(90)}]$ (i.e. in the centre of the distribution). Therefore, it can be concluded that Eq. (4) is quite accurate for the cases under consideration.

The model was then calibrated by running 5 simulations for different values of the fracture toughness, $\mathcal{G}_c^{(p)}$, with $p = 0.1, 25, 50, 75, 99.9$ to which corresponded 5 values of lambda $\lambda_p = \bar{X}/\sqrt{\mathcal{G}_c^{(p)}}$. All the cases of Tab. 1 were considered. The values were then fitted using a PCHIP to calculate $\Phi(\lambda)$ of Eq. (3). The numerical values and best fits are shown in Fig. 4.

Determining $\Phi(\lambda)$ allows us to define the emulator. Numerical simulations (Fig. 5) were performed for different combinations of strength and fracture toughness equally spaced in the ranges $[X^{(0.1)}, X^{(99.9)}]$ and $[\mathcal{G}_c^{(0.1)}, \mathcal{G}_c^{(99.9)}]$. Considering the joint distribution of strength and fracture toughness defined in the domain $[X^{(0.1)}, X^{(99.9)}] \cap [\mathcal{G}_c^{(0.1)}, \mathcal{G}_c^{(99.9)}]$ the error is calculated to be less than 2% at the centre of the distribution (i.e. $[X^{(10)}, X^{(90)}] \cap [\mathcal{G}_c^{(10)}, \mathcal{G}_c^{(90)}]$) and less than 10% elsewhere, thus allowing considering the emulator sufficiently accurate.

¹In this case the classical percentile formula is used. KDE fitting is not necessary since numerous points ($N = 1000$) are available.

Note that calibration must be performed for each specimen configuration (e.g. for different layouts, geometries, load types, etc.). The fact that calibration only requires 5 simulations justifies the strategy of training separate emulators of each configuration.

3.2. *Statistic analysis and derivation of the design allowables*

If the distribution of strength and fracture toughness were known, the statistical analysis would be trivial. Assuming, for example, the distributions to be log-normal with parameters defined in Tab. 3 it will be sufficient to run a MCS analysis providing as input material properties values sampled from the said distributions and derive the distribution of the structural strength for each specimen. This will allow determining all the statistical parameters of the structural strength distribution, including the mean value, the standard deviation, or the first percentile (Fig. 6).

But the strength and fracture toughness distributions (Fig. 7) are unknown to the design engineers. They only rely on experimental values that can be seen as realization of the said distributions.

To explain the procedure suggested for the determination of the A-basis value, we sample the experimental values from the said distributions (indicated with crosses in Fig. 7) and reported in Tab. 4) and assume that these are the only data available to the design engineers.

The suggested procedure is the following:

- Knowing the experimental values of the strength, the reference value can be calculated as the mean value, therefore $\bar{X} = \frac{1}{n_X} \sum X_i$.
- Knowing the maximum and minimum values of fracture toughness, five equally spaced values of the fracture toughness are chosen in the $[\mathcal{G}_c^{\min}, \mathcal{G}_c^{\max}]$ interval.
- Running the computational model² using as input parameters the reference value of the strength \bar{X} and the 5 values of fracture toughness (5 simulations in total) permits calibrating the emulator.

²Although it might be obvious to the reader, it should be stressed the fact that the computational model does not depend on the distributions of the strength and fracture toughness but only on the values of the reference strength \bar{X} and fracture toughness \mathcal{G}_c used for its calibration. In Sec. 3.1 a log-normal distributions for strength and fracture toughness were implicitly assumed for the sake of discussion.

- Using the procedure reported in Sec. 2.3 the structural strength distributions and the corresponding statistics (in particular, the A-basis value) are obtained.

Figs. 8 and 9 report the distribution obtained for the 1st percentile of the structural strength, $f^{(1)}$ for the tensile and compressive cases, respectively. For each specimen is reported not only the $f^{(1)}$ distribution, but also the true $f^{(1)}$ value (ignored by the design engineers but known and calculated by us and reported in Fig. 6), the predicted value of $f^{(1)}$ and the A-basis value, computed as the expected value and the 5th percentile of the $f^{(1)}$ distribution.

A quick inspection of Figs. 8 and 9 reveals that the prediction for $f^{(1)}$ (mean value of the distribution) underestimates and overestimates the true value in tension and compression, respectively. One might wonder what causes this behaviour and the answer is straightforward: it mainly depends on the (mock) experimental data (Tab. 4) that fed the model.

To assess the influence of the material parameters provided as input, one might compute the A-basis value for different sets of material parameters and compare the distribution of the A-basis value with $f^{(1)}$. These calculations were performed for 200 different sets of material parameters (randomly generated by sampling from the strength and fracture toughness distributions). Analysing their results (Figs. 10 and 11) one observes that, depending on the material parameters in input, the A-basis value prediction might be conservative (lower than $f^{(1)}$) or not (larger than $f^{(1)}$). The integral of the A-basis distributions for values lower than $f^{(1)}$ provides the probability of getting a conservative prediction, P_c , reported in Figs. 10 and 11, which ranges between 86 and 98% and between 83 and 91% for the tensile and compressive cases, respectively. It is concluded that the proposed methodology delivers consistent predictions.

A quick examination of the data reveals that non-conservative predictions are related to sets of material parameters that overestimate the strength and/or the fracture toughness of the material. The way to reduce the probability of getting non-conservative predictions is to enhance the quality of the experimental data. Consequently, this emphasises the need for improved experimental characterisation procedures.

To evaluate the accuracy of the emulator, the A-basis value (and possibly other statistics) could be estimated by computing the structural strength for different combinations of the strength and fracture toughness and bootstrapping these values to build the structural

strength distribution. For the experiments of Tab. 4 this would mean performing 72 and 70 simulations³ for tension and compression, respectively. This number is sensibly higher than what is required for calibrating the emulator but still manageable, especially if an HPC infrastructure is available. Note that this approach also permits performing uncertainty quantification when an emulator is not available.

This exercise was conducted for two specimens: OHT24 and OHC24. The $f^{(1)}$ distributions (Fig. 12) obtained using the two approaches (emulator and bootstrap, EB; and bootstrap only, BO) provide close predictions. The EB distribution appears to be shifted towards the left, thus providing more conservative predictions. This phenomenon depends exclusively on the emulator that tends to underestimate the structural strength f as the values of the strength grow smaller (see also the lower graphs in Figs. 3a and 3b).

Note that for the compressive case (Fig. 12b) the EB approach provides a non-conservative prediction of the A-basis value (even though it is only by 3 MPa!) and that this circumstance, as previously mentioned, depends only on the set of material properties used for the calculation.

4. Conclusions

The main concluding remarks of the present work can be summarised as follows:

- A methodology was developed for performing uncertainty quantification for advanced progressive damage models for composites. The QoI was the structural strength and the associated statistics.
- An efficient emulator was defined for unnotched and open hole specimens in tension and compression, making a number of simplified assumptions. Comparing the emulator's and the computational model's predictions permits reaching the conclusion that the proposed emulator is sufficiently accurate.
- A bootstrapping technique was used to predict the distribution of the structural strength. This allows determining the desired statistics such as expected value, standard deviation, skewness, and kurtosis.

³10 values of strength and 8 of fracture toughness are available in tension. Since a strength value is repeated twice, the unique values are 9. Therefore, the necessary simulations are 72 instead of 80.

- Bootstrapping notably fails when used to determine extreme values, as the first percentile of the strength distribution required for calculating the A-basis value. For this reason, the calculation of the first percentile was performed on an analytical expression of the structural strength distribution obtained by KDE fitting.
- Distributions for ply strength and fracture toughness were assumed, and the distribution of the structural strength was computed. This allowed the calculation of the true value of the 1st percentile of the distribution. Without assuming any distribution, the distribution of the 1st percentile of the structural strength was computed employing the bootstrapping methodology proposed. The predicted 1st percentile and the calculated A-basis value were in excellent agreement with the true $f^{(1)}$.
- Distributions of the 1st percentile of the structural strength were obtained using two approaches requiring i) the use of the emulator and bootstrap (EB), and ii) the use of bootstrap only. Their predictions agree well.
- The emulator is able to provide systematically conservative results. Non-conservative predictions are obtained for material parameters that provide a poor statistical characterisation of the actual strength and fracture toughness distributions.
- A total of 5 simulations were used for the emulator’s calibration, a negligible amount compared with other approaches. This fact makes the proposed methodology particularly suitable for use in an industrial environment to speed up the certification process.

References

- [1] A. Needleman, A continuum model for void nucleation by inclusion debonding, *J Appl Mech* 54 (3) (1987) 525–531.
- [2] Y. Mi, M. A. Crisfield, G. A. O. Davies, H. B. Hellweg, Progressive delamination using interface elements, *J Compos Mater* 32 (14) (1998) 1246–1272.
- [3] G. Alfano, M. A. Crisfield, Finite element interface models for the delamination analysis of laminated composites: mechanical and computational issues, *Int J Numer Methods Eng* 50 (7) (2001) 1701–1736.

- [4] P. P. Camanho, C. G. Davila, M. F. de Moura, Numerical simulation of mixed-mode progressive delamination in composite materials, *J Compos Mater* 37 (16) (2003) 1415–1438.
- [5] A. Turon, P. Camanho, J. Costa, C. Dávila, A damage model for the simulation of delamination in advanced composites under variable-mode loading, *Mech Mater* 38 (11) (2006) 1072–1089.
- [6] A. Turon, P. P. Camanho, J. Costa, J. Renart, Accurate simulation of delamination growth under mixed-mode loading using cohesive elements: Definition of interlaminar strengths and elastic stiffness, *Compos Struct* 92 (8) (2010) 1857–1864.
- [7] G. Catalanotti, C. Furtado, T. Scalici, G. Pitarresi, F. van der Meer, P. Camanho, The effect of through-thickness compressive stress on mode ii interlaminar fracture toughness, *Compos Struct* 182 (2017) 153–163.
- [8] C. Schuecker, H. E. Pettermann, A continuum damage model for fiber reinforced laminates based on ply failure mechanisms, *Compos Struct* 76 (1) (2006) 162–173.
- [9] P. Maimí, P. P. Camanho, J. A. Mayugo, C. G. Dávila, A continuum damage model for composite laminates: Part i – constitutive model, *Mech Mater* 39 (10) (2007) 897–908.
- [10] P. Maimí, P. P. Camanho, J. A. Mayugo, C. G. Dávila, A continuum damage model for composite laminates: Part ii – computational implementation and validation, *Mech Mater* 39 (10) (2007) 909–919.
- [11] J. Reinoso, G. Catalanotti, A. Blázquez, P. Areias, P. Camanho, F. París, A consistent anisotropic damage model for laminated fiber-reinforced composites using the 3d-version of the puck failure criterion, *Int J Solids Struct* 126-127 (2017) 37–53.
- [12] F. P. van der Meer, C. Oliver, L. J. Sluys, Computational analysis of progressive failure in a notched laminate including shear nonlinearity and fiber failure, *Compos Sci Technol* 70 (4) (2010) 692–700.
- [13] E. V. Iarve, M. R. Gurvich, D. H. Mollenhauer, C. A. Rose, C. G. Dávila, Mesh-independent matrix cracking and delamination modeling in laminated composites, *Int J Numer Methods Eng* 88 (8) (2011) 749–773.
- [14] M. Vogler, R. Rolfes, P. P. Camanho, Modeling the inelastic deformation and fracture of polymer composites – part i: Plasticity model, *Mech Mater* 59 (2013) 50–64.
- [15] P. Camanho, M. Bessa, G. Catalanotti, M. Vogler, R. Rolfes, Modeling the inelastic

- deformation and fracture of polymer composites – Part II: Smearred crack model, *Mech Mater* 59 (2013) 36–49.
- [16] L. Varandas, G. Catalanotti, A. Melro, R. Tavares, B. Falzon, Micromechanical modelling of the longitudinal compressive and tensile failure of unidirectional composites: The effect of fibre misalignment introduced via a stochastic process, *Int J Solids Struct* 203 (2020) 157–176.
- [17] L. F. Varandas, G. Catalanotti, A. R. Melro, B. G. Falzon, On the importance of nesting considerations for accurate computational damage modelling in 2d woven composite materials, *Comput Mater Sci* 172 (2020) 109323.
- [18] C. Furtado, G. Catalanotti, A. Arteiro, P. Gray, B. Wardle, P. Camanho, Simulation of failure in laminated polymer composites: Building-block validation, *Compos Struct* 226 (2019) 111168.
- [19] D. Dalli, L. Varandas, G. Catalanotti, S. Foster, B. Falzon, Assessing the current modelling approach for predicting the crashworthiness of formula one composite structures, *Compos B Eng* 201 (2020) 108242.
- [20] S. T. Pinho, P. Robinson, L. Iannucci, Fracture toughness of the tensile and compressive fibre failure modes in laminated composites, *Compos Sci Technol* 66 (13) (2006) 2069–2079.
- [21] G. Catalanotti, J. Xavier, P. Camanho, Measurement of the compressive crack resistance curve of composites using the size effect law, *Compos - A: Appl Sci Manuf* 56 (2014) 300–307.
- [22] G. Catalanotti, A. Arteiro, M. Hayati, P. Camanho, Determination of the mode i crack resistance curve of polymer composites using the size-effect law, *Eng Fract Mech* 118 (2014) 49–65.
- [23] G. Catalanotti, J. Xavier, Measurement of the mode ii intralaminar fracture toughness and r-curve of polymer composites using a modified iosipescu specimen and the size effect law, *Eng Fract Mech* 138 (2015) 202–214.
- [24] R. Pinto, G. Catalanotti, P. Camanho, Measuring the intralaminar crack resistance curve of fibre reinforced composites at extreme temperatures, *Compos - A: Appl Sci Manuf* 91 (2016) 145–155.
- [25] P. Kuhn, G. Catalanotti, J. Xavier, P. Camanho, H. Koerber, Fracture toughness and

- crack resistance curves for fiber compressive failure mode in polymer composites under high rate loading, *Compos Struct* 182 (2017) 164–175.
- [26] P. Kuhn, G. Catalanotti, J. Xavier, M. Ploeckl, H. Koerber, Determination of the crack resistance curve for intralaminar fiber tensile failure mode in polymer composites under high rate loading, *Compos Struct* 204 (2018) 276–287.
- [27] G. Catalanotti, P. Kuhn, J. Xavier, H. Koerber, High strain rate characterisation of intralaminar fracture toughness of gfrps for longitudinal tension and compression failure, *Compos Struct* 240 (2020) 112068.
- [28] D. Dalli, G. Catalanotti, L. Varandas, B. Falzon, S. Foster, Mode i intralaminar fracture toughness of 2d woven carbon fibre reinforced composites: A comparison of stable and unstable crack propagation techniques, *Eng Fract Mech* 214 (2019) 427–448.
- [29] G. Catalanotti, P. Camanho, J. Xavier, C. Dávila, A. Marques, Measurement of resistance curves in the longitudinal failure of composites using digital image correlation, *Compos Sci Technol* 70 (13) (2010) 1986–1993.
- [30] R. Cappello, G. Pitarresi, J. Xavier, G. Catalanotti, Experimental determination of mode i fracture parameters in orthotropic materials by means of digital image correlation, *Theor Appl Fract Mech* 108 (2020) 102663.
- [31] B. Sudret, S. Marelli, J. Wiart, Surrogate models for uncertainty quantification: An overview, in: 2017 11th European Conference on Antennas and Propagation (EUCAP), 2017, pp. 793–797.
- [32] C. Soize, R. Ghanem, Physical systems with random uncertainties: Chaos representations with arbitrary probability measure, *SIAM J Sci Comput* 26 (2) (2004) 395–410.
- [33] K. Konakli, B. Sudret, Polynomial meta-models with canonical low-rank approximations: Numerical insights and comparison to sparse polynomial chaos expansions, *J Comput Phys* 321 (2016) 1144–1169.
- [34] C. E. Rasmussen, C. K. I. Williams, *Gaussian Processes for Machine Learning*, The MIT Press, 2005.
- [35] A. J. Smola, B. Schölkopf, A tutorial on support vector regression, *Stat Comput* 14 (3) (2004) 199–222.
- [36] O. P. Le Maître, O. M. Knio, H. N. Najm, R. G. Ghanem, A stochastic projection method for fluid flow: I. basic formulation, *J Comput Phys* 173 (2) (2001) 481–511.

- [37] D. Xiu, *Numerical Methods for Stochastic Computations: A Spectral Method Approach*, Princeton University Press, 2010.
- [38] M. Berveiller, B. Sudret, M. Lemaire, Stochastic finite element: a non intrusive approach by regression, *Eur J Comput Mech* 15 (1-3) (2006) 81–92.
- [39] G. Blatman, B. Sudret, Adaptive sparse polynomial chaos expansion based on least angle regression, *J Comput Phys* 230 (6) (2011) 2345–2367.
- [40] C. Furtado, L. Pereira, R. Tavares, M. Salgado, F. Otero, G. Catalanotti, A. Arteiro, M. Bessa, P. Camanho, A methodology to generate design allowables of composite laminates using machine learning, *Int J Solids Struct* 233 (2021) 111095.
- [41] S. Pouresmaeeli, B. Falzon, Uncertainty quantification of pure and mixed mode interlaminar fracture of fibre-reinforced composites via a stochastic reduced order model, *Compos Struct* 278 (2021) 114683.
- [42] S. Ranftl, G. M. Melito, V. Badeli, A. Reinbacher-K ostinger, K. Ellermann, W. von der Linden, Bayesian uncertainty quantification with multi-fidelity data and gaussian processes for impedance cardiography of aortic dissection, *Entropy* 22 (1) (2020). doi:10.3390/e22010058.
URL <https://www.mdpi.com/1099-4300/22/1/58>
- [43] B. Efron, R. J. Tibshirani, *An Introduction to the Bootstrap*, no. 57 in *Monographs on Statistics and Applied Probability*, Chapman & Hall/CRC, Boca Raton, Florida, USA, 1993.
- [44] M. Chernick, *Bootstrap Methods: A Guide for Practitioners and Researchers*, Wiley Series in Probability and Statistics, Wiley, 2011.
- [45] F. Pedregosa, G. Varoquaux, A. Gramfort, V. Michel, B. Thirion, O. Grisel, M. Blondel, P. Prettenhofer, R. Weiss, V. Dubourg, J. Vanderplas, A. Passos, D. Cournapeau, M. Brucher, M. Perrot, E. Duchesnay, Scikit-learn: Machine learning in Python, *Journal of Machine Learning Research* 12 (2011) 2825–2830.

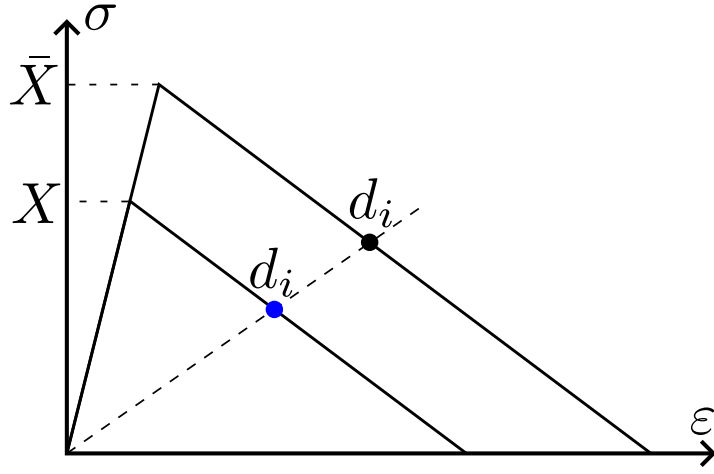


Figure 1: Softening laws with same λ .

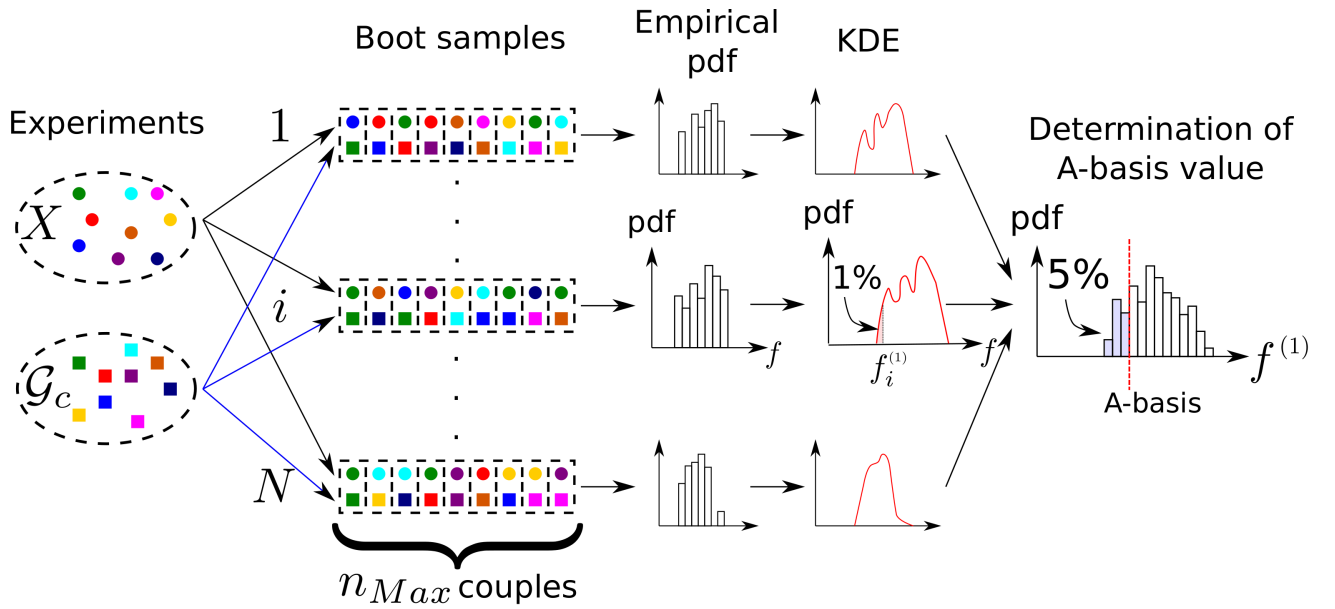
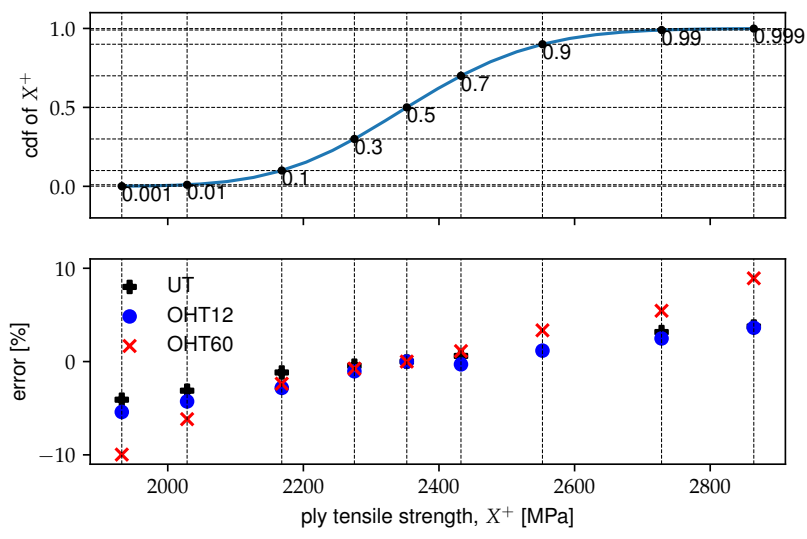
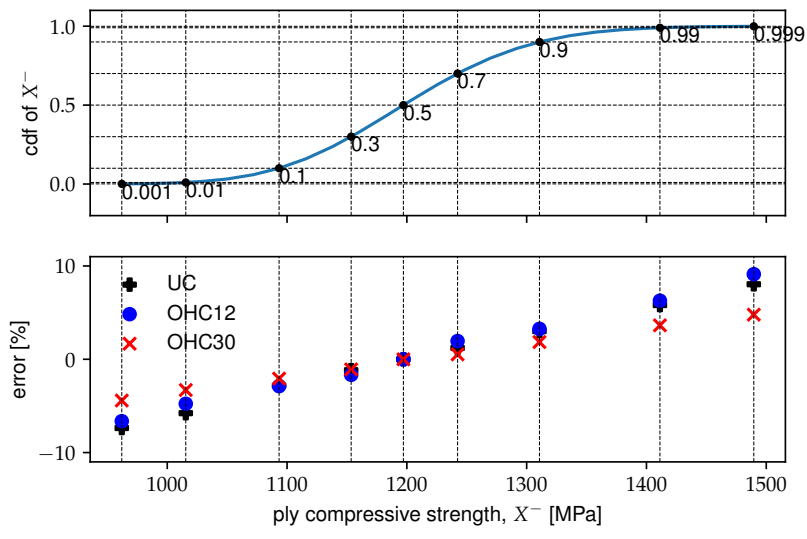


Figure 2: Statistical analysis.

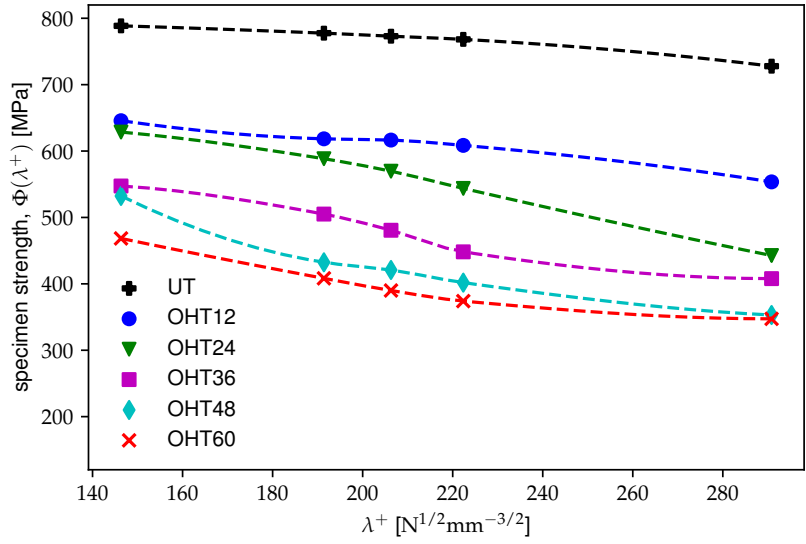


(a) Tension

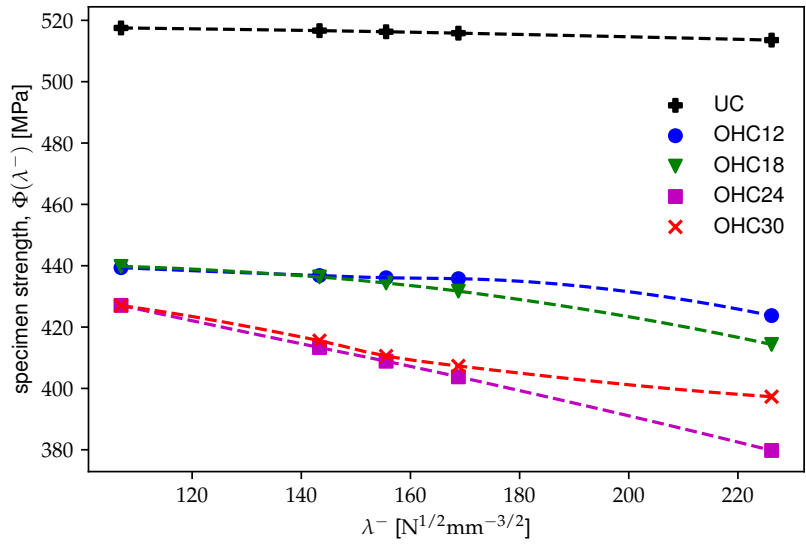


(b) Compression

Figure 3: Error between the emulator's and computational model's predictions.

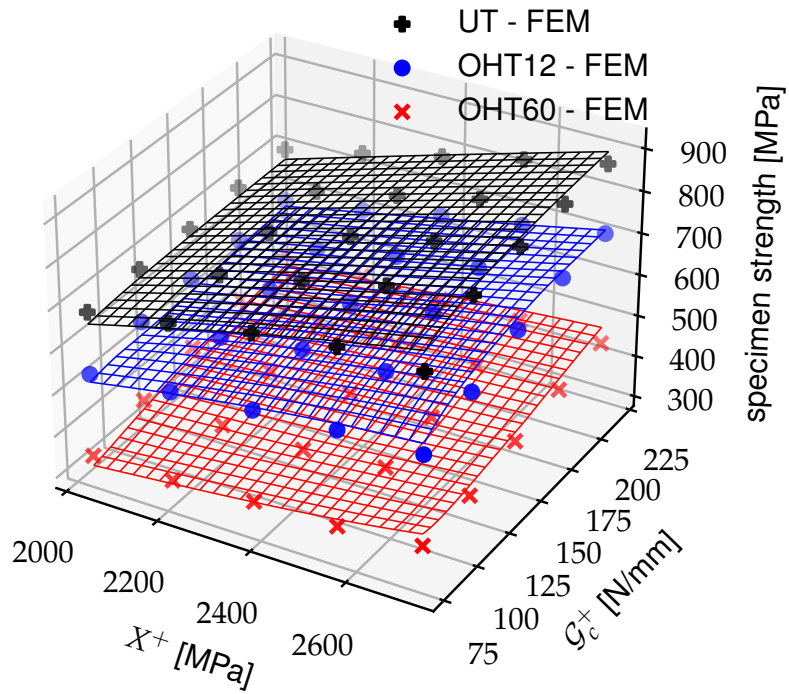


(a) Tension

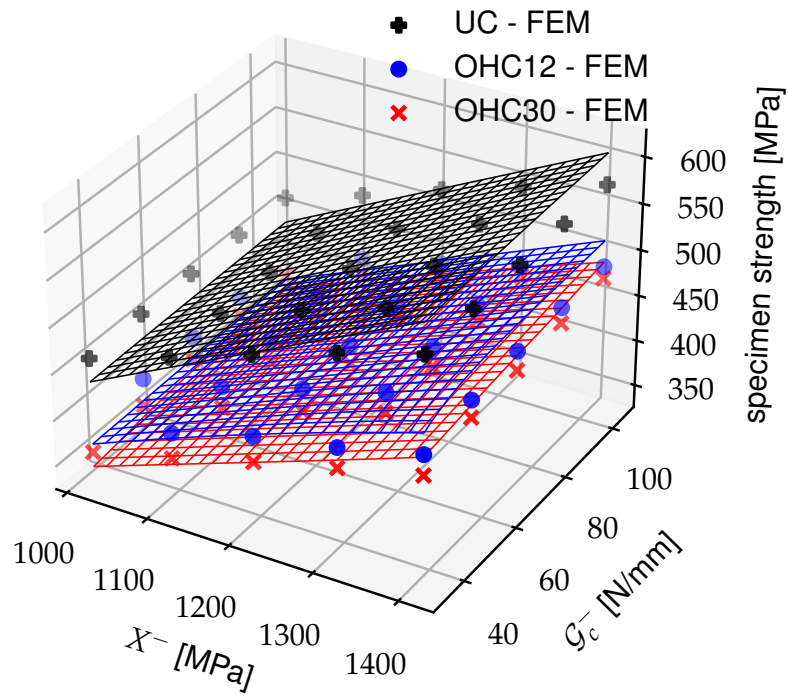


(b) Compression

Figure 4: Calibration: numerical simulations and PCHIP interpolations for $\Phi(\lambda)$.

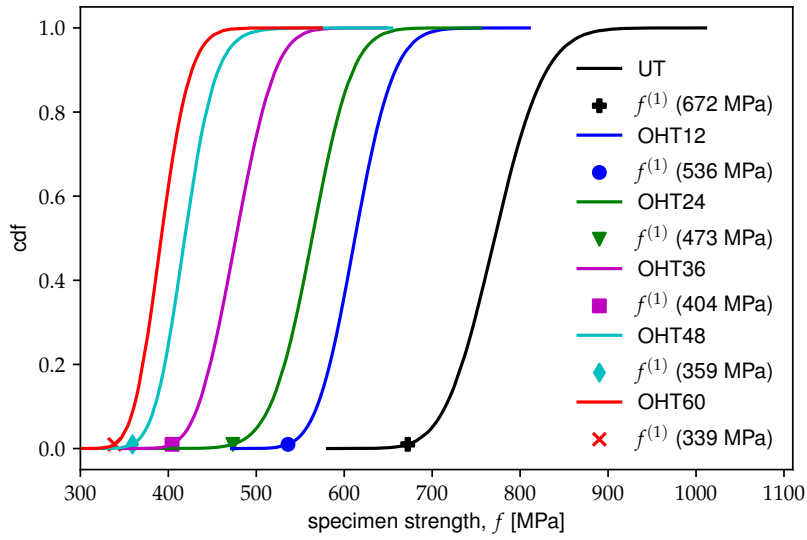


(a) Tension

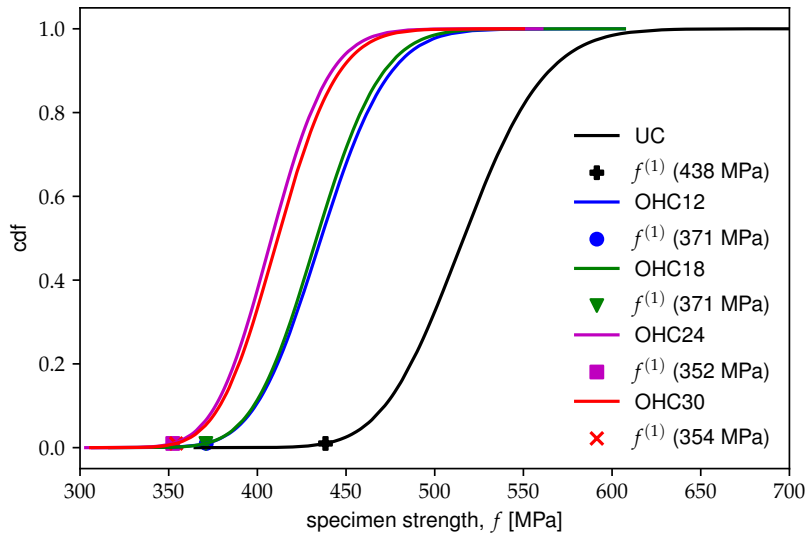


(b) Compression

Figure 5: Computational model's (scatter points) and emulator's (wired surface) predictions.

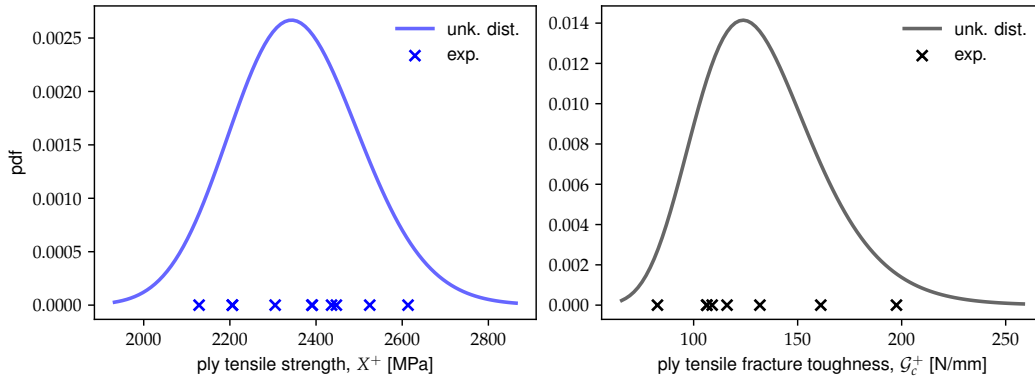


(a) Tension

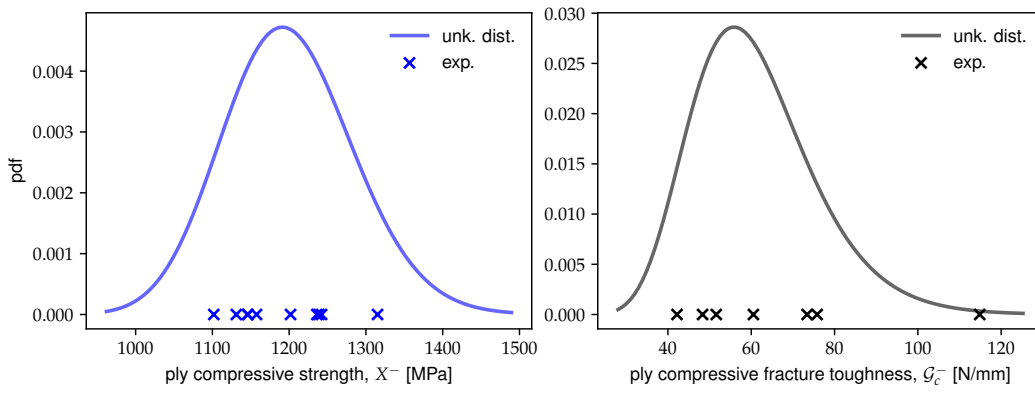


(b) Compression

Figure 6: Cumulative density functions (CDFs) and first percentile for the structural strength distribution.



(a) Tension



(b) Compression

Figure 7: Distribution of the strength and fracture toughness and mock experimental data.

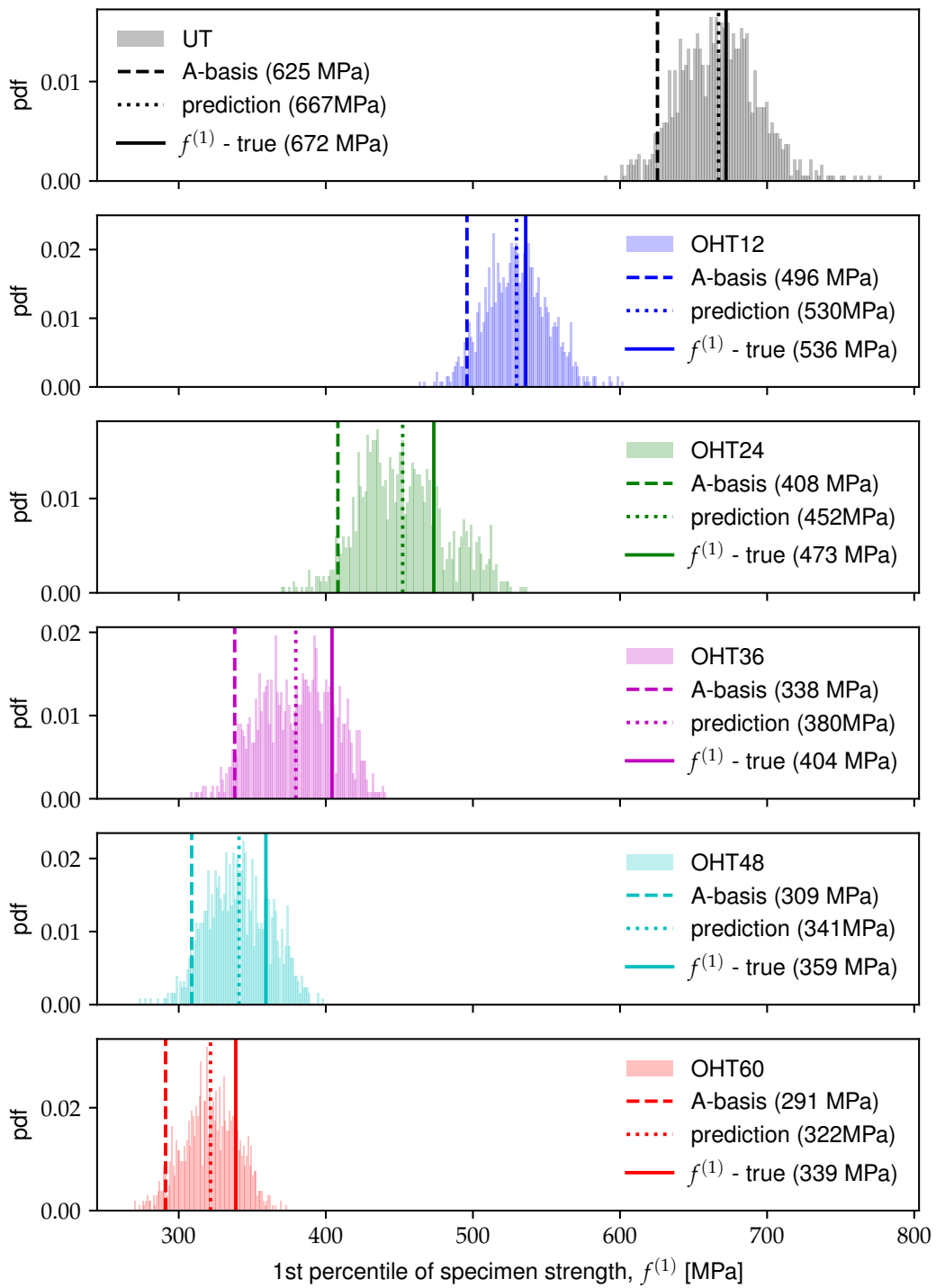


Figure 8: Distribution of the 1st percentile of the structural strength for the tensile case.

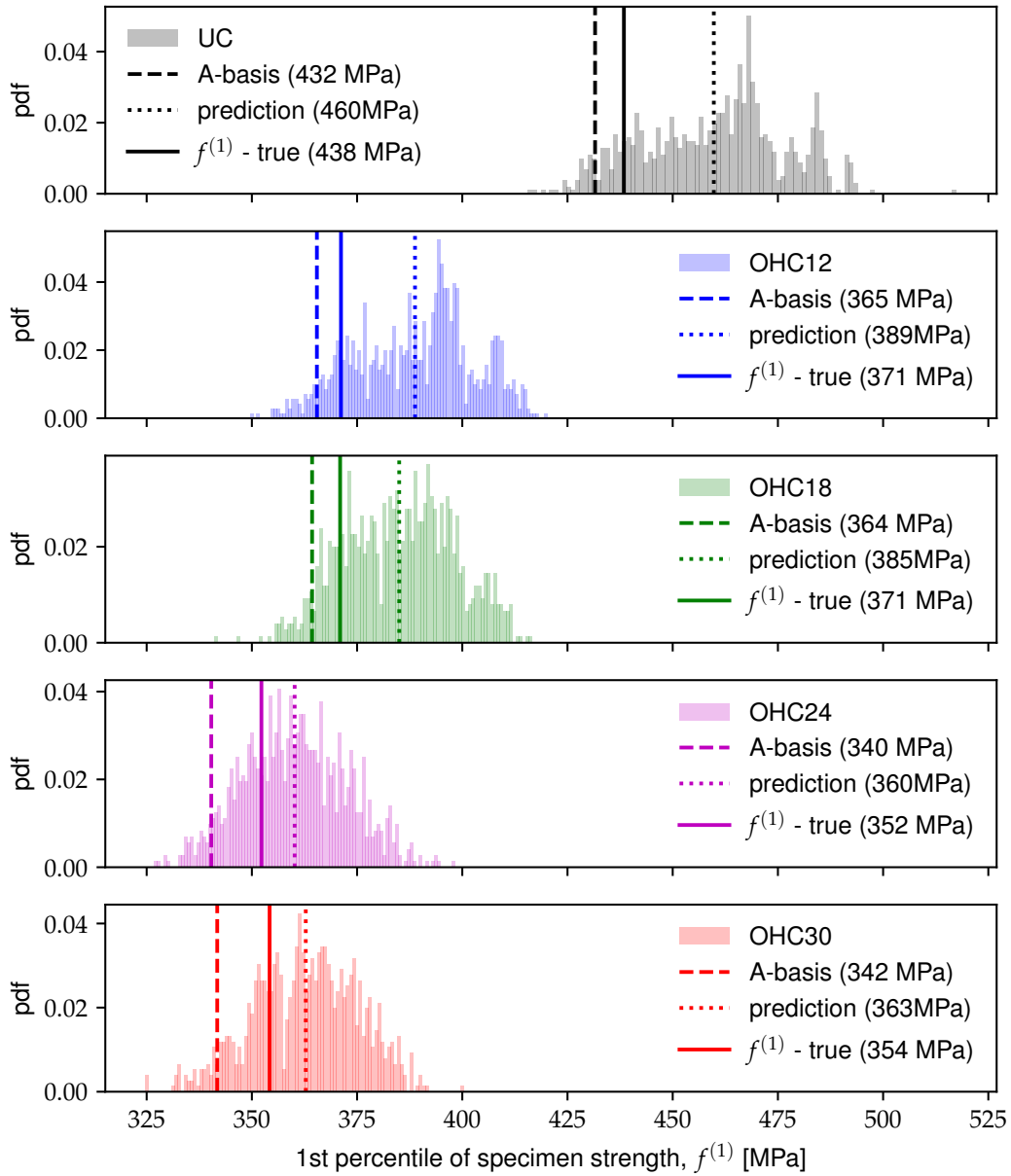


Figure 9: Distribution of the 1st percentile of the structural strength for the compressive case.

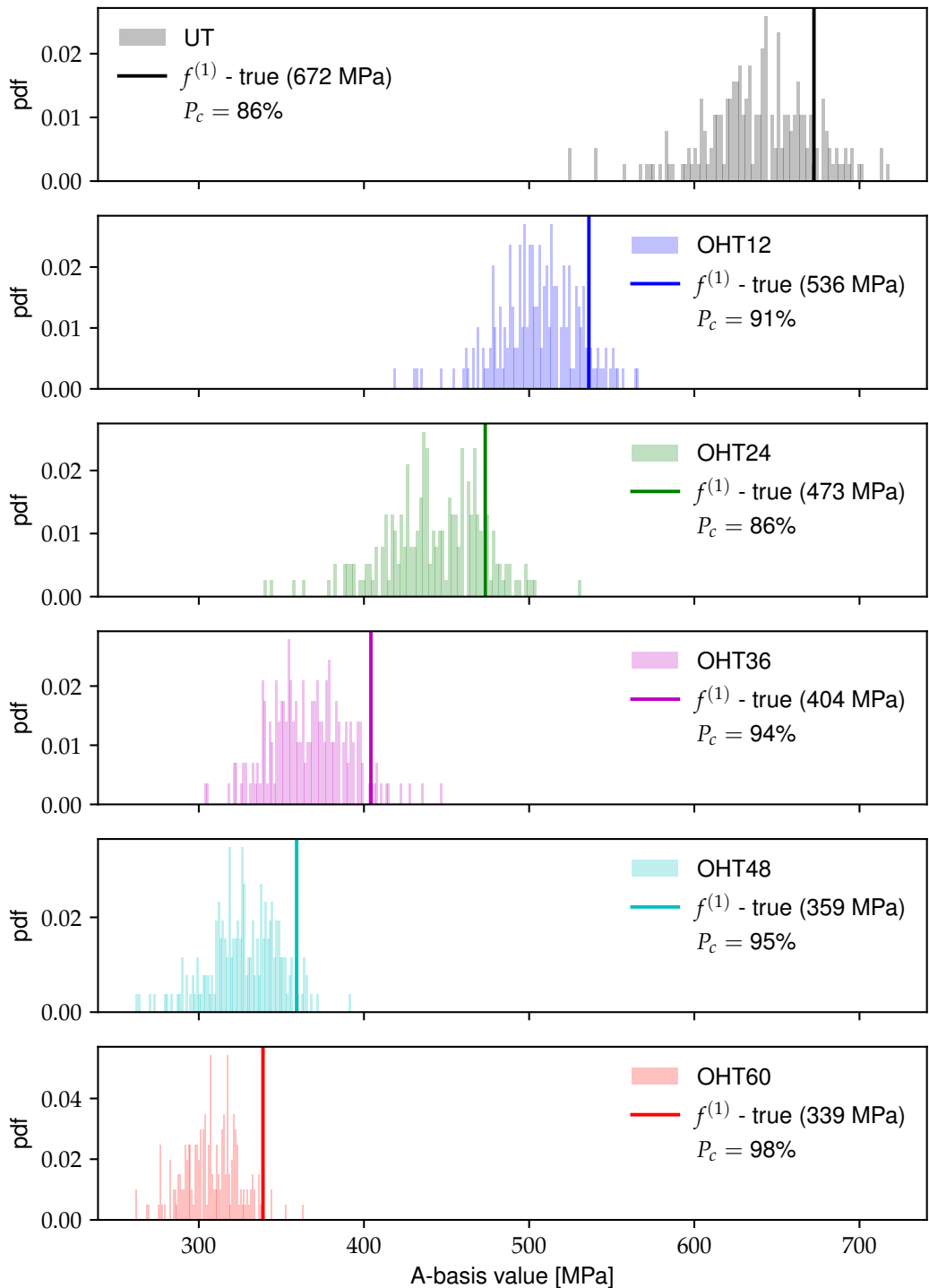


Figure 10: Distribution of the A-basis value for the tensile case.

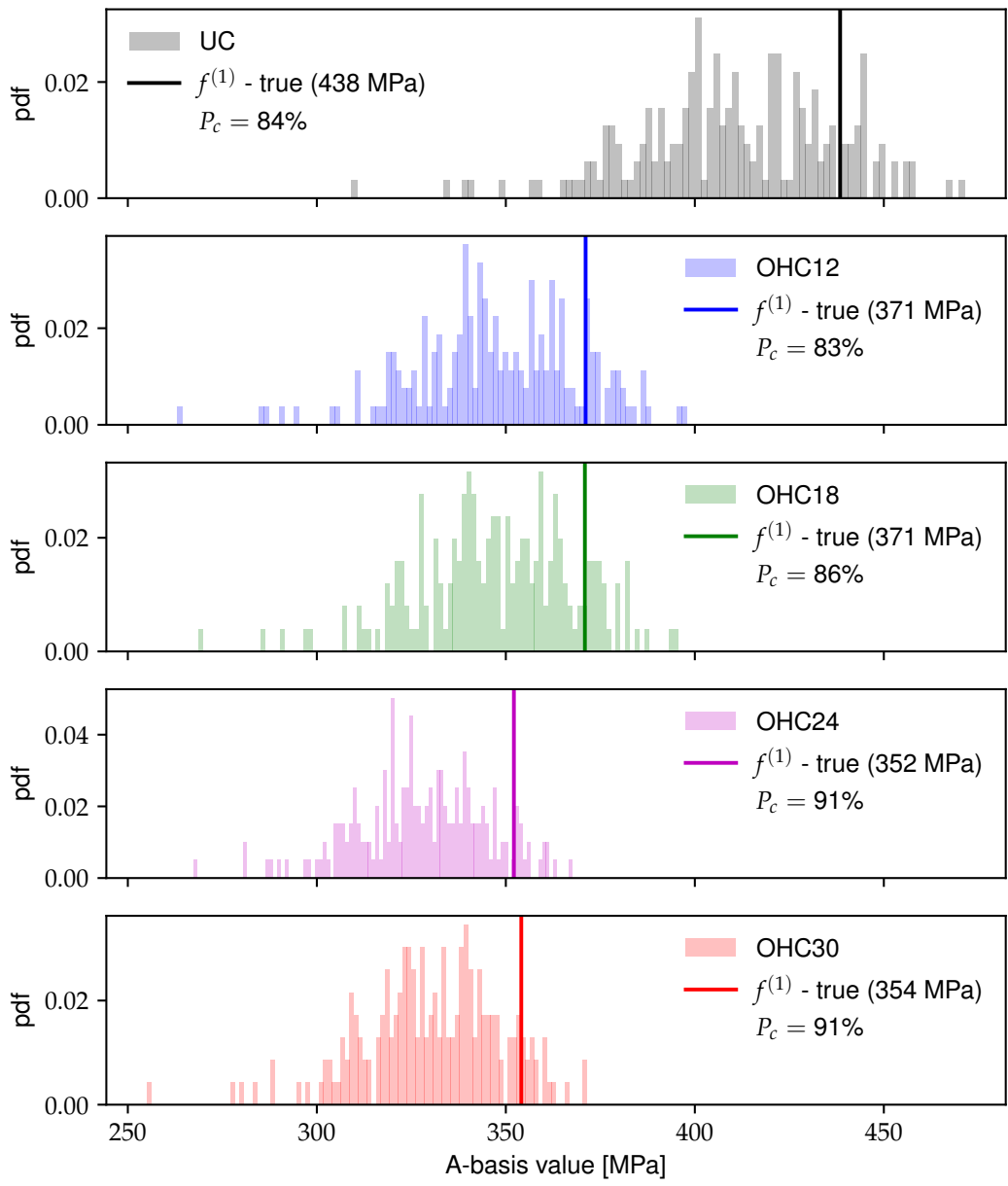
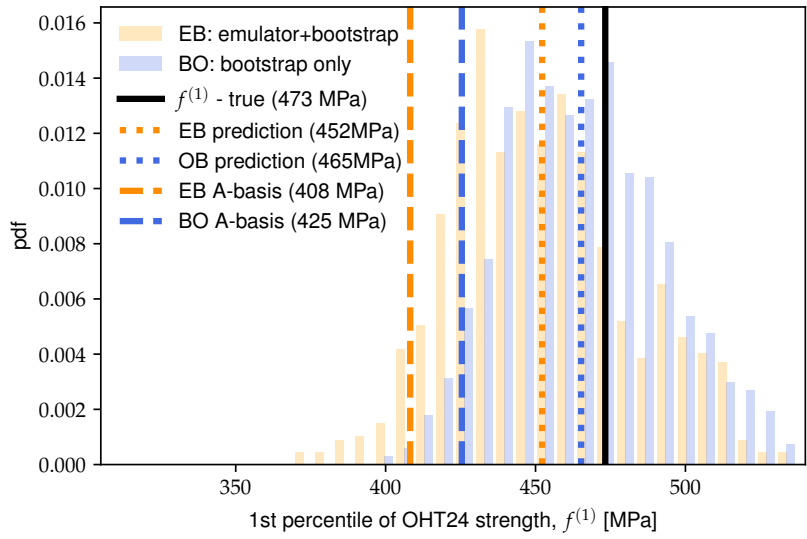
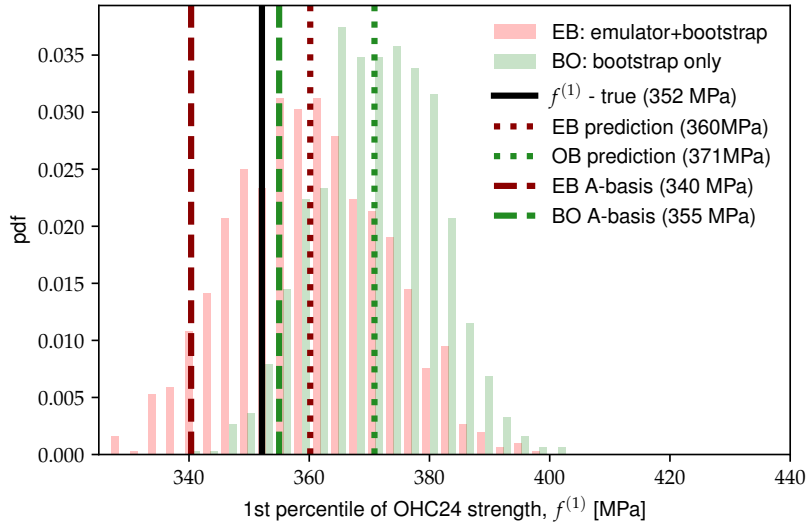


Figure 11: Distribution of the A-basis value for the compressive case.



(a) Tension



(b) Compression

Figure 12: Comparison between EB and BO approaches.

Table 1: Virtual experiments

Specimen	Specimen Label	Thickness (mm)	Width (mm)	Hole Diameter (mm)
In tension				
Unnotched Tension	UT	3	20	–
Open Hole Tension	OHT12	3	12	2
	OHT24	3	24	4
	OHT36	3	36	6
	OHT48	3	48	8
	OHT60	3	60	10
In compression				
Unnotched Compression	UC	3	20	–
Open Hole Compression	OHC12	3	12	2
	OHC18	3	18	3
	OHC24	3	24	4
	OHC30	3	30	5

Table 2: Material properties

Material Property	Symbol	Units	Value
Geometry of the ply			
Elemental / Ply thickness	t	mm	125
UD fracture angle under uniaxial compression	α_0	rad	0.925
Elastic properties of the ply			
Young's modulus for longitudinal tension	E_1	MPa	171420
Young's modulus for transverse tension	E_2	MPa	9080
In-plane shear modulus	G_{12}	MPa	5290
Major Poisson's coefficient	ν_{12}	–	0.32
Strength of the ply			
Longitudinal tensile strength	X^+	MPa	2323.5
Normalised longitudinal tensile stress at the inflection point	f_X^+	–	0.4
Longitudinal compressive strength	X^-	MPa	1200.1
Normalised longitudinal compression stress at inflection point	f_X^-	–	0.2
Transverse tensile strength	Y^+	MPa	62.3
Transverse compressive strength	Y^-	MPa	253
Biaxial transverse tensile strength	Y_B^+	MPa	38.7
Biaxial transverse compressive strength	Y_B^-	MPa	600
In-plane shear strength	S_L	MPa	92.3
Shear stress that activates plastic flow	S_L^p	MPa	66.9
Shear incremental stiffness under plastic flow	K_p	–	0.08
Fracture toughness of the ply			
Fracture toughness for longitudinal tension	\mathcal{G}_1^+	kJ/m ²	133.3
Normalised dissipated energy up to the inflection point	f_G^+	–	0.3
Fracture toughness for longitudinal compression	\mathcal{G}_1^-	kJ/m ²	61
Mode I fracture toughness for transverse tension	\mathcal{G}_2^+	kJ/m ²	0.28
Mode I fracture toughness for transverse compression	\mathcal{G}_2^-	kJ/m ²	1.31
Mode II fracture toughness	\mathcal{G}_6	kJ/m ²	0.79
Interlaminar properties			
Penalty stiffness	K	N/mm ³	106
Strength under pure mode I	τ_N	MPa	62.3
Strength under pure mode II	τ_{sh}	MPa	92.3
Mode I fracture toughness	\mathcal{G}_{Ic}	kJ/m ²	0.28
Mode II fracture toughness	\mathcal{G}_{IIc}	kJ/m ²	0.79
Benzeggagh-Kenane mixed-mode interaction parameter	η_{BK}	–	1.45
Friction coefficient	μ	–	0.1

Table 3: Stochastic material properties

Material Properties	Parameter	Symbol	Units	Value
In tension				
Longitudinal tensile strength	Mean Value	$\mu(X^+)$	MPa	2323.5
	Standard deviation	$\sigma(X^+)$	MPa	150.3
	Scale parameter	μ_X^+	MPa	7.76
	Shape parameter	σ_X^+	MPa	0.064
Fracture toughness for longitudinal tension	Mean Value	$\mu(\mathcal{G}_1^+)$	kJ/m ²	133.3
	Standard deviation	$\sigma(\mathcal{G}_1^+)$	kJ/m ²	30.0
	Scale parameter	$\mu_{\mathcal{G}}^+$	kJ/m ²	4.87
	Shape parameter	$\sigma_{\mathcal{G}}^+$	kJ/m ²	0.22
In compression				
Longitudinal compressive strength	Mean Value	$\mu(X^-)$	MPa	1200.1
	Standard deviation	$\sigma(X^-)$	MPa	85.0
	Scale parameter	μ_X^-	MPa	7.09
	Shape parameter	σ_X^-	MPa	0.071
Fracture toughness for longitudinal compression	Mean Value	$\mu(\mathcal{G}_1^-)$	kJ/m ²	61.0
	Standard deviation	$\sigma(\mathcal{G}_1^-)$	kJ/m ²	15.0
	Scale parameter	$\mu_{\mathcal{G}}^-$	kJ/m ²	4.08
	Shape parameter	$\sigma_{\mathcal{G}}^-$	kJ/m ²	0.24

Table 4: Mock experimental data for the A-basis value calculation.

X^+ (MPa)	\mathcal{G}_c^+ (N/mm)	X^- (MPa)	\mathcal{G}_c^- (N/mm)
2305.1	82.6	1201.8	114.8
2613.5	197.5	1242.2	42.2
2447.1	161.1	1146.3	51.6
2390.3	108.9	1236.0	60.5
2205.8	106.3	1315.1	75.8
2205.8	106.4	1238.6	48.3
2128.5	116.1	1131.2	73.4
2524.6	131.9	1157.5	
2391.2		1145.7	
2436.1		1101.8	